Supplement of Atmos. Chem. Phys., 21, 5137–5149, 2021
https://doi.org/10.5194/acp-21-5137-2021-supplement

Atmospheric Chemistry and Physics
Open Access
EGU

Supplement of

Characterization of secondary organic aerosol from heated-cooking-oil emissions: evolution in composition and volatility

Manpreet Takhar et al.

Correspondence to: Arthur W. H. Chan (arthurwh.chan@utoronto.ca)

Table S1: Description of the experiments conducted in this study.

Exp.	Canola oil SOA ($\mu g\ m^{-3}$)	OH exposure (molecules cm^{-3} s)	Photochemical age (h)[a]
1	26.57±2.32	5.77×10^{10}	10.7
2	75.67±5.33	6.43×10^{10}	11.9
3	93.48±13.1	7.07×10^{10}	13.1
4	151.46±12.45	8.01×10^{10}	14.8
5	108.74±17.6	8.60×10^{10}	15.9
6	207.2±11.91	9.23×10^{10}	17.1
7	2670.4±170.85	2.20×10^{11}	40.7

a: calculated by assuming an average atmospheric OH concentration of 1.5×10^6 molecules cm^{-3} (Mao et al., 2009).

Table S2: List of all the model compounds used in this study to recreate 73 along with its $f_{M\text{-}15/73}$. SIMPOL.1 (Pankow and Asher, 2008) vapor pressure and its corresponding saturation concentrations are also listed for the compounds quantified in this study.

#	Carbon #	Molecular weight (MW)	Derivatized MW (M)	M-15	$f_{M\text{-}15/73}$ (NIST)	$f_{M\text{-}15/73}$ (MS detector response)	Vapor pressure (atm)	Saturation concentration ($\mu g\ m^{-3}$)
				2-COOH				
1	3	104	248	233	0.147	0.128±0.03	3.5E-07	29.5
2	4	118	262	247	0.24	0.273±0.06	1.3E-07	3.2[a]
3	5	132	276	261	0.67	0.254±0.1	4.9E-08	54.8[a]
4	6	146	290	275	0.198	0.143±0.04	1.9E-08	0.8[a]
5	7	160	304	289	0.187	0.198±0.07	7.0E-09	4.2[a]
6	8	174	318	303	0.147	0.182±0.08	2.6E-09	0.09[a]
7	9	188	332	317	0.268	0.313±0.22	9.9E-10	0.5[a]
				2-COOH + 1-OH				
8	3	120	336	321	0.029	0.062±0.014	2.3E-09	0.19
9	4	134	350	335	0.067	0.051±0.03	8.6E-10	0.02
10	5	148	364	349	0.146	0.141±0.05	3.2E-10	0.36
11	6	162	378	363	0.106[a1]	0.072±0.03	1.2E-10	5.3E-03
12	6	162	378	363	0.178[a2]	0.272±0.11	1.2E-10	5.3E-03
13	7	176	392	377	0.012	0.034±0.02	4.6E-11	2.7E-02

14	8	190	406	391	0.002	n/a	6.5E-12	6.4E-04
15	9	204	420	405	n/a	n/a	2.4E-12	3.2E-03
1-COOH + 2-OH								
16	3	106	322	307	0.04	0.058±0.01	4.9E-08	400.2
17	4	120	336	321	0.116	0.052±0.04	1.8E-08	150.6
18	5	134	350	335	n/a	n/a	6.9E-09	56.7
19	6	148	364	349	n/a	0.125±0.05	2.6E-09	21.3
20	7	162	378	363	n/a	0.019±0.01	9.8E-10	8.02
21	7	162	378	363	n/a	0.026±0.01	9.8E-10	8.02
22	7	162	378	363	n/a	0.068±0.01	9.8E-10	8.02
23	7	162	378	363	n/a	0.056±0.01	9.8E-10	8.02
24	8	176	392	377	n/a	0.023±0.02	3.7E-10	3.01
25	8	176	392	377	n/a	0.026±0.01	3.7E-10	3.01
26	9	190	406	391	n/a	0.033±0.02	1.4E-10	1.1
27	9	190	406	391	n/a	0.021±0.02	1.4E-10	1.1
2-COOH + 2-OH								
28	4	150	438	423	0.07	0.029±0.002	5.7E-12	1.4E-04
29	5	164	452	437	0.059	0.057±0.01	2.1E-12	2.4E-03
30	6	178	466	451	0.05	n/a	8.0E-13	3.5E-05
1-COOH + 1-OH								
31	2	76	220	205	0.123	0.11±0.01	1.9E-05	162375.7
32	3	90	234	219	0.479	0.48±0.15	7.5E-06	61085.0
33	4	104	248	233	0.024[b1]	0.053±0.02	2.8E-06	22979.9
34	4	104	248	233	0.226[b2]	0.099±0.05	2.8E-06	22979.9
35	4	104	248	233	0.179[b3]	0.147±0.06	2.8E-06	22979.9
36	5	118	262	247	0.043[c1]	0.034±0.01	1.1E-06	8644.9
37	5	118	262	247	0.06[c2]	0.064±0.01	1.1E-06	8644.9
38	5	118	262	247	0.341[c3]	0.245±0.12	1.1E-06	8644.9
39	6	132	276	261	0.04[d1]	0.043±0.01	3.9E-07	3252.2
40	6	132	276	261	0.089[d2]	0.068±0.02	3.9E-07	3252.2
41	6	132	276	261	0.215[d3]	0.106±0.06	3.9E-07	3252.2

42	7	146	290	275	0.06	0.071±0.01	1.5E-07	1223.5
43	8	160	304	289	0.109	0.05±0.008	5.6E-08	460.3
44	9	174	318	303	0.074	n/a	2.1E-08	173.1
				1-COOH				
45	6	116	188	173	0.69	0.604±0.05	6.1E-05	5.7
46	7	130	202	187	1.18	0.656±0.02	2.3E-05	5.3
47	8	144	216	201	1.14	0.769±0.06	8.6E-06	4.8
48	9	158	230	215	1.24	0.815±0.04	3.2E-06	4.4
49	10	172	244	229	1.02	0.947±0.11	1.2E-06	3.9

a: Bilde et al. (2003).
a1: positional isomers
a2: positional isomers
b1: α-hydroxyisobutyric acid
b2: β-hydroxybutyric acid
b3: 3-hydroxybutyric acid
c1: α-hydroxyvaleric acid
c2: β-hydroxy-n-valeric acid
c3: 4-hydroxyvaleric acid
d1: 4-methyl 2-keto pentanoic acid
d2: 3-hydroxycaproic acid
d3: 5-hydroxyhexanoic acid

Table S3: List of all the model compounds used in this study to recreate 73 for single precursor oxidation experiments along with corresponding product molar yields.

M-15	**Heptanal + OH**	**2-heptenal + OH**	**2-octenal + OH**	**2,4-heptadienal + OH**	**2,4-decadienal + OH**
OH exposure (molec cm^{-3} s)[a]	7.71×10^{10}	6.2×10^{10}	6.02×10^{10}	5.34×10^{10}	5.72×10^{10}
OH reaction rate constant (cm^3 $molec^{-1}$ s^{-1})	3.0×10^{-11}[b]	4.4×10^{-11}[c]	4.1×10^{-11}[d]	4.6×10^{-10}[e]	4.6×10^{-10}[f]
			1-COOH + 1-OH		
205	1.87E-07	7.38E-05	4.44E-05	9.40E-05	1.94E-05
219	6.85E-08	1.26E-05	1.29E-05	3.84E-06	1.74E-06
233	3.67E-06	2.97E-05	2.45E-05	2.66E-05	2.24E-06
247	4.49E-06	5.82E-05	5.03E-05	3.77E-05	4.52E-06
261	3.73E-06	4.78E-05	2.22E-05	0	9.07E-07

275	6.69E-06	4.35E-06	6.46E-06	0	0
289	0	5.70E-07	2.27E-05	0	7.30E-07
303	0	0	0	0	0
317	0	0	0	0	0
		2-COOH			
233	1.96E-06	5.32E-06	9.26E-06	7.44E-06	4.05E-06
247	5.56E-06	2.35E-05	3.02E-05	1.98E-05	1.02E-05
261	1.82E-05	7.85E-05	9.24E-05	5.26E-05	3.0E-05
275	2.87E-06	5.00E-06	3.62E-06	5.20E-06	9.31E-06
289	3.19E-06	9.94E-07	1.34E-05	0	5.92E-07
303	0	0	0	0	0
317	0	0	0	0	0
		2-COOH + 1-OH			
321	0	0	0	0	5.45E-06
335	3.11E-06	0	0	2.96E-05	1.76E-05
349	1.33E-05	3.02E-05	4.20E-05	2.61E-05	1.07E-05
363	2.29E-05	1.80E-05	7.28E-05	0	4.29E-06
377	1.63E-06	1.38E-06	1.72E-05	1.45E-05	1.46E-06
391	0	0	0.00016	0	0
		2-COOH + 2-OH			
423	0	1.69E-06	1.90E-06	3.81E-06	2.18E-05
437	0	2.15E-06	2.73E-06	5.97E-07	2.28E-06
451	0	2.93E-06	0	9.19E-07	2.72E-06
		1-COOH + 2-OH			
307	3.41E-07	3.32E-06	0	1.06E-05	4.95E-06
321	4.27E-06	3.82E-05	2.31E-05	0	5.09E-06
335	0	0	0	0	0
349	5.50E-06	0	6.69E-05	0	7.46E-06
363	0	4.42E-05	2.68E-05	4.86E-06	0
377	0	0	0	0	5.71E-06
391	0	0	0	0	0

		1-COOH			
173	3.70E-06	0	4.53E-05	0	8.99E-06
187	0	1.65E-06	2.64E-06	1.73E-06	1.09E-05
201	0	0	1.05E-06	0	6.0E-06
215	0	0	0	0	4.37E-07
229	0	0	0	0	3.33E-06

a: as calculated from the decay of cyclopentane in each set of experiment.
b: Atkinson and Arey (2003).
c: Davis et al. (2007).
d: Gao et al. (2009).
e: calculated by multiplying 2-heptenal OH reaction rate constant by a factor of 105 as obtained from Kwok & Atkinson (1995).
f: assumed same as 2,4-heptadienal.

Section 1. Sample calculation for aldehyde reaction timescales

The reaction rate constant of methacrolein is obtained from Atkinson and Arey (2003) and is as follows:

k_{OH} = 2.9E-11 cm^3 $molec^{-1}$ s^{-1}

k_{O3} = 1.2E-18 cm^3 $molec^{-1}$ s^{-1}

For lowest OH exposure at 5.77×10^{10} molecules cm^{-3} s, OH conc = 2.88×10^{8} molecules cm^{-3}, and ozone concentration was measured ~0.5 ppm which corresponds to 1.23×10^{13} molecules cm^{-3} assuming 1ppb O_3 = 2.46×10^{10} molecules cm^{-3}. At these photooxidation conditions, methacrolein reaction timescale is calculated as follows:

$$\tau_{OH} = \frac{1}{k_{OH}[OH]} = \sim 120\ s$$

$$\tau_{O_3} = \frac{1}{k_{O_3}[O_3]} = 1129\ min$$

For highest OH exposure at 2.2×10^{11} molecules cm^{-3} s, OH conc = 1.1×10^{9} molecules cm^{-3}, and ozone concentration was measured ~12.6 ppm which corresponds to 3.1×10^{14} molecules cm^{-3}. At these photooxidation conditions, methacrolein reaction timescale is calculated as:

$$\tau_{OH} = 31\ s$$

$$\tau_{O_3} = \sim 45\ min$$

Section 2. Chemical characterization using TD-GC/MS

Gas-phase analysis: Tenax tubes were desorbed in the thermal desorption system (TDS) for thermal desorption with initial temperature at 50 °C held for 2 minutes followed by a ramp of 60 °C min^{-1} to 320 °C and held for 4 minutes. The analytes were transferred to the cooling injection system (CIS4, Gerstel) via a transfer line maintained at 300 °C during the run. The CIS4 was embedded with quartz wool filled quartz liner maintained at -40 °C during thermal

desorption, and was heated to 320 °C at 12 °C s^{-1}, and held for 5 minutes at 320 °C. The GC column was held for 2 minutes at 40 °C and heated to 250 °C at a rate of 7 °C min^{-1} and held for additional 5 minutes at 250 °C.

Particle-phase analysis: 4 mm diameter filter punches were inserted into glass tubes (6 mm OD × 178 mm length, Gerstel) and placed in the TDS for thermal desorption. The temperature ramping program for thermal desorption was from 40 °C initial temperature held for 2 minutes followed by a ramp of 60 °C min^{-1} to 320 °C and held for 5 minutes at 320 °C. After the analytes were desorbed in the TDS, they were transferred to the cooling injection system (CIS4, Gerstel) via a transfer line maintained at 300 °C during the run. The CIS4 was embedded with quartz wool filled quartz liner maintained at 10 °C during thermal desorption to preconcentrate the desorbed analytes. The CIS was heated from 10 °C to 320 °C at 12 °C s^{-1}, and held for an additional 7 minutes at 320 °C. The GC column was heated from 40 °C to 300 °C at a ramp of 10 °C min^{-1} and held for 5 minutes at 300 °C. All samples were analyzed under electron impact at 70 eV using a standard tungsten filament with a source temperature at 230 °C. The MS was operated at 3.1 scans s^{-1} with an acquisition range from mass-to-charge (*m/z*) ratio 35 to 500.

Section 3. Procedure to recreate *m/z* 73

Step 1: Extract all model M-15 ions from the total ion chromatogram.

Step 2: Divide each M-15 ion with its corresponding $f_{M-15,73}$. Wherever, NIST $f_{M-15,73}$ was not available, $f_{M-15,73}$ was calculated from the instrument detector response.

Step 3: Since higher *m/z* ions are susceptible to fragmentation under high electron ionization efficiency (70 eV in our study), therefore caution must be taken in recreating M-15 ions so as to avoid double counting of actual (or real) peaks. An example of this scenario is shown in Fig. S4 (a), using an example chromatogram of *m/z* 233, 335 and 349. As shown in Fig. S4 (a), *m/z* 233 has large number of fragments from higher *m/z* ions, and some of these fragments belong to actual *m/z*. Peaks at retention time (RT) = 13.059 min corresponds to *m/z* 335 while at RT = 14.599 min belongs to *m/z* 349. Therefore, in order not to overestimate these peaks, fragments of higher *m/z* should be set to zero when recreating smaller *m/z*.

Step 4: Repeat step 3 iteratively for remaining M-15 ions to minimize the effect of double counting, and only accounting for signal from actual or real peaks as shown in Fig. S4 (b).

Step 5: Add all M-15 together to recreate 73 as shown in Fig. 2 (main text) with scatter plot shown in Fig. S4 (c).

Section 4. Sample calculation for Sect. 3.3.1 (formation of particle-phase oxidation products)

Estimation of SOA formation potential using product yields of VOC precursor oxidation products were done as follows:

M-15 ion = 219 corresponds to 3-hydroxypropanoic acid has a yield of 1.26E-05 upon photooxidation of 2-heptenal which is used to estimate SOA formation for canola oil photooxidation using Eq. (4) in main text.

Where, γ_{ij} represents yields of products (i) from photooxidation of 2-heptenal (j) (obtained from Table S3), and ΔVOC_j represents the decay in concentration of 2-heptenal during photooxidation of canola oil vapors, and was calculated based on the measured OH exposure.

Therefore, for 3-hydroxypropanoic acid (or M-15 = 219) the SOA formation can be predicted as:

$SOA_{pred} = \quad 1.26\text{E} - 05 * 299 * 90 = 0.339$ µg m^{-3}.

Similarly, using above methodology SOA formation can be estimated from other VOC precursors such as heptanal, 2-octenal, 2,4-heptadienal, and 2,4-decadienal.

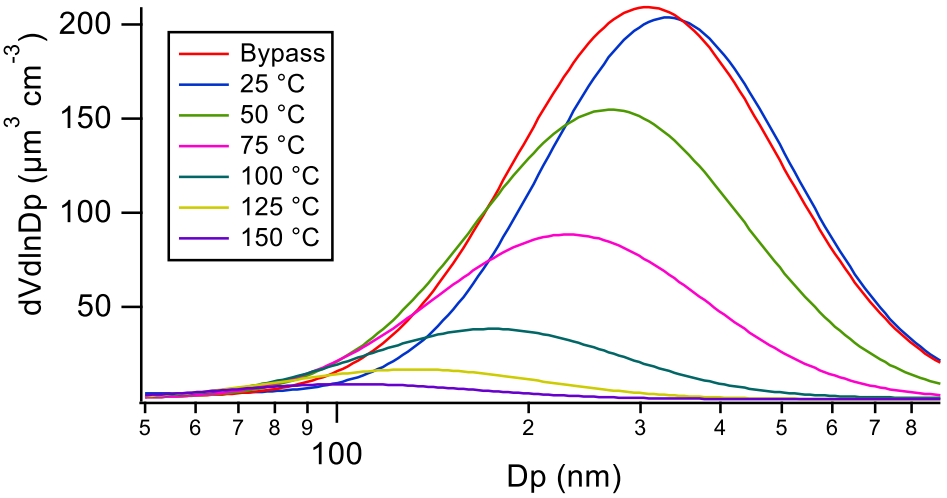

Figure S1. Particle volume distribution of canola oil SOA at an OH exposure of 9.23×10^{10} molecules cm^{-3} s measured by SMPS when subject to heating in a thermodenuder. The volume mode diameter shifts from 332 nm at 25 °C to 106 nm at 150 °C corresponding to a decrease in volume concentration of ~96%.

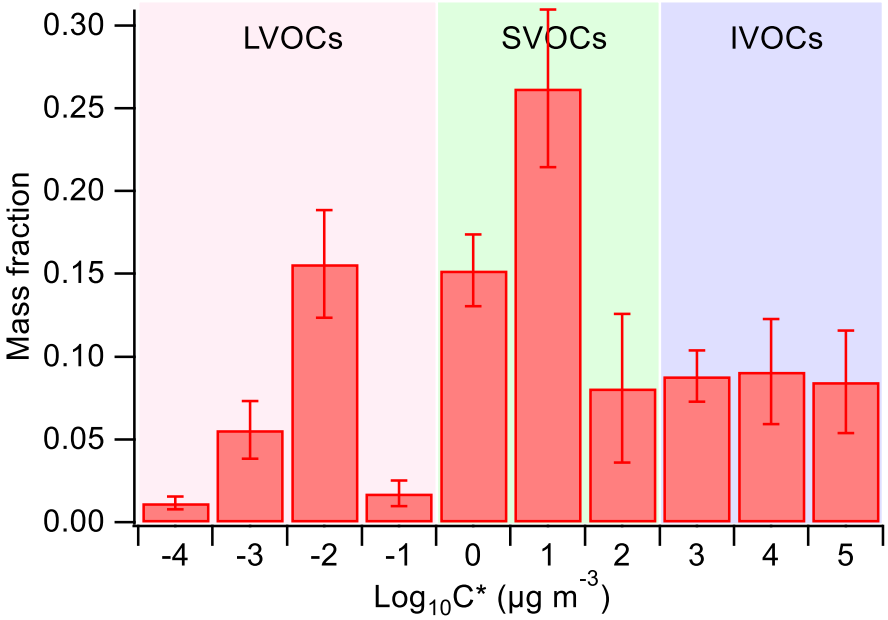

Figure S2. Volatility distribution of canola oil SOA at an OH exposure of 9.23×10^{10} molecules cm^{-3} s. The volatility distribution corresponds to 24% mass in LVOCs, ~50% in SVOCs, and 26% in IVOCs. The error bars represent ±1σ.

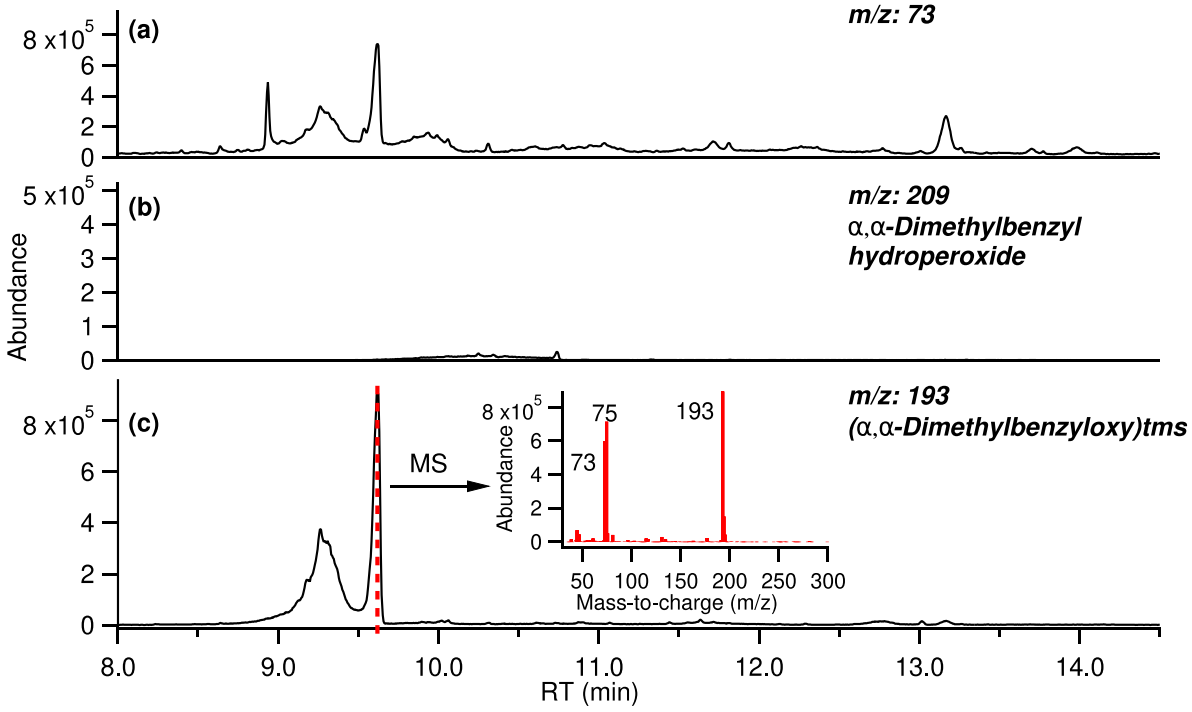

Figure S3. Chromatogram of cumene hydroperoxide upon *in situ* derivatization (a). Based on the analytical technique discussed in main text, extracted M-15 (*m/z* = 209) chromatogram of cumene hydroperoxide contains no peaks as shown in panel (b), instead the derivatized form of R-OH is observed as shown in panel (c) along with its mass spectrum shown in the inset.

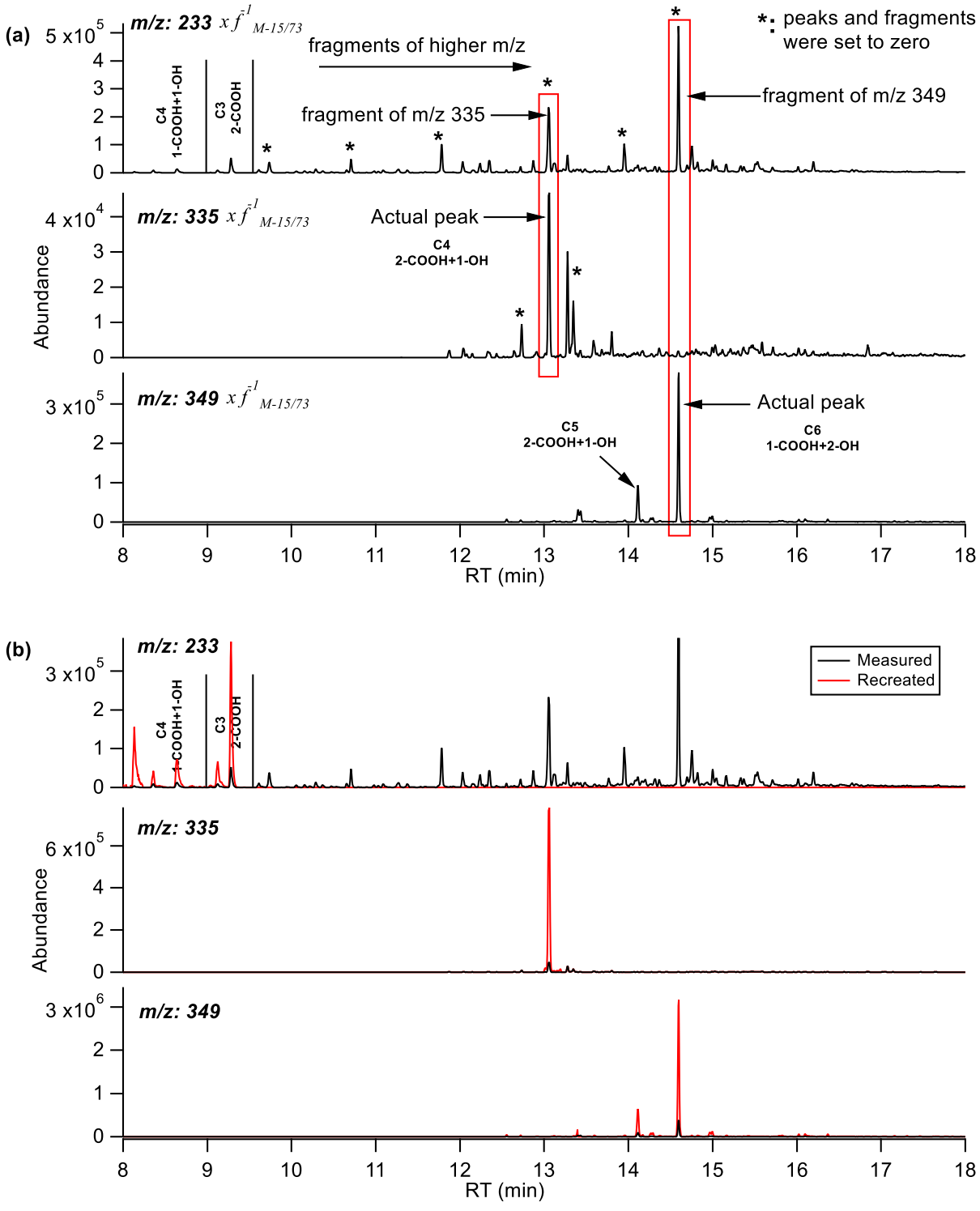

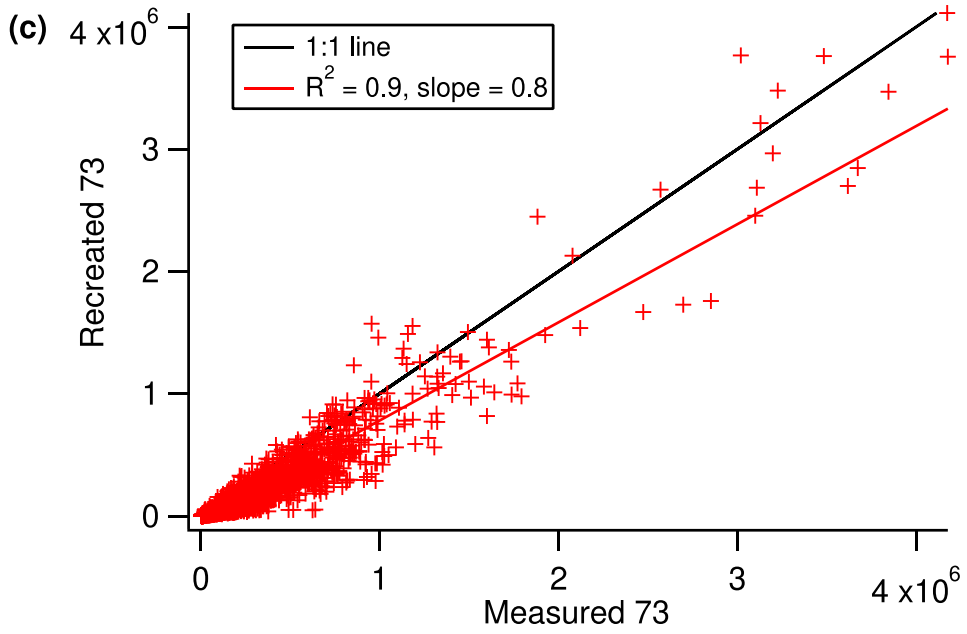

Figure S4. Illustration to recreate *m/z* 73. (a) shows the unprocessed M-15 chromatograms obtained from canola oil photooxidation highlighting that lower *m/z* ions are susceptible to interference from higher *m/z*, therefore appropriate processing (refer to Sect. 3, step 3) of chromatograms should be carried out to account for these interferences. (b) chromatograms obtained after cleaning of fragments from each model *m/z*. (c) total ion chromatogram of measured and recreated 73.

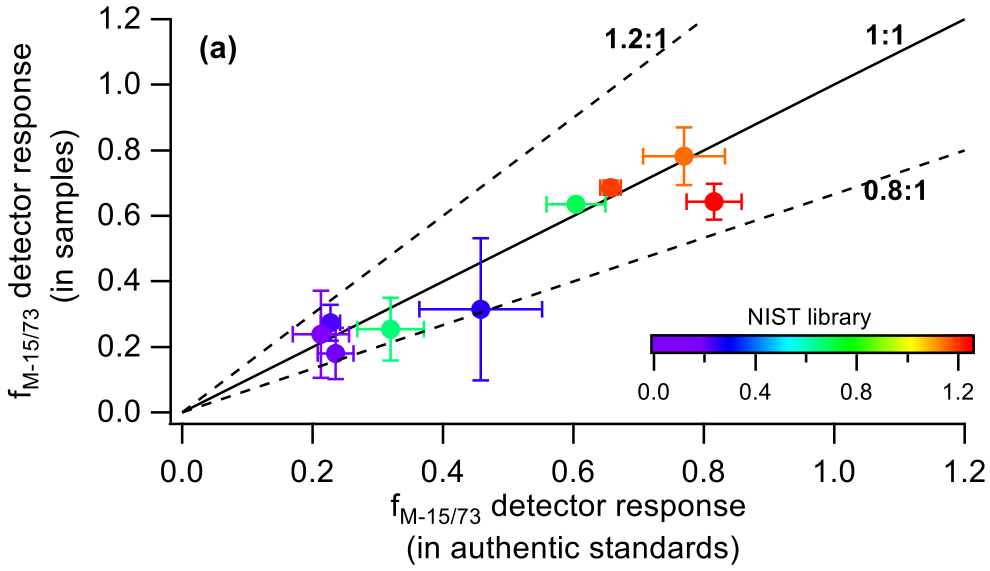

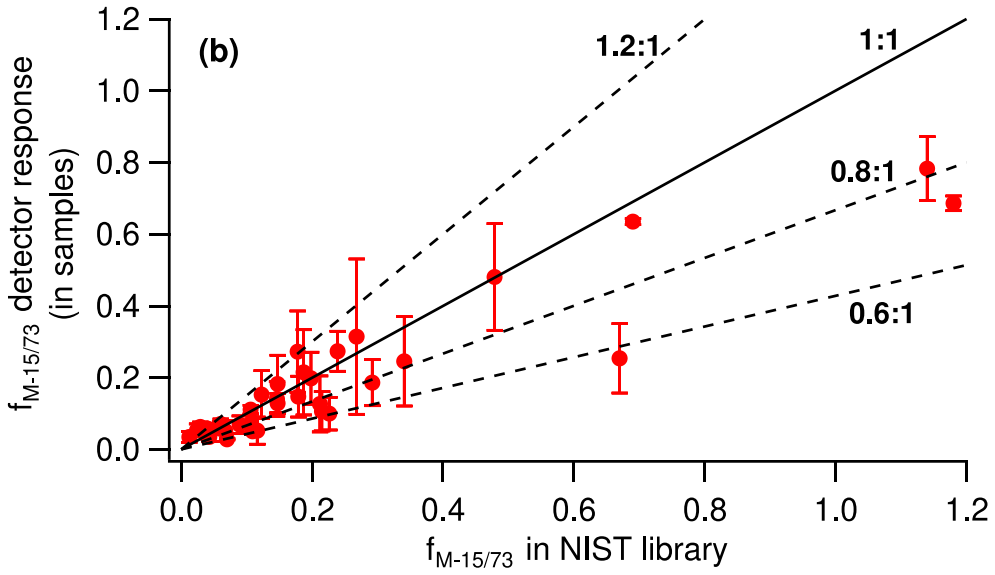

Figure S5. Calculated uncertainties in pseudo molecular ion fraction of model components. (a) compares $f_{M-15/73}$ from instrument detector response in samples vs that in authentic standards colour coded with $f_{M-15/73}$ available in NIST library. (b) shows the comparison of $f_{M-15/73}$ obtained from instrument detector response to that available in NIST library. Both comparisons show that the uncertainty in measurement of $f_{M-15/73}$ is within 20% for measured compounds except for tartaric acid which is within 40% uncertainty.

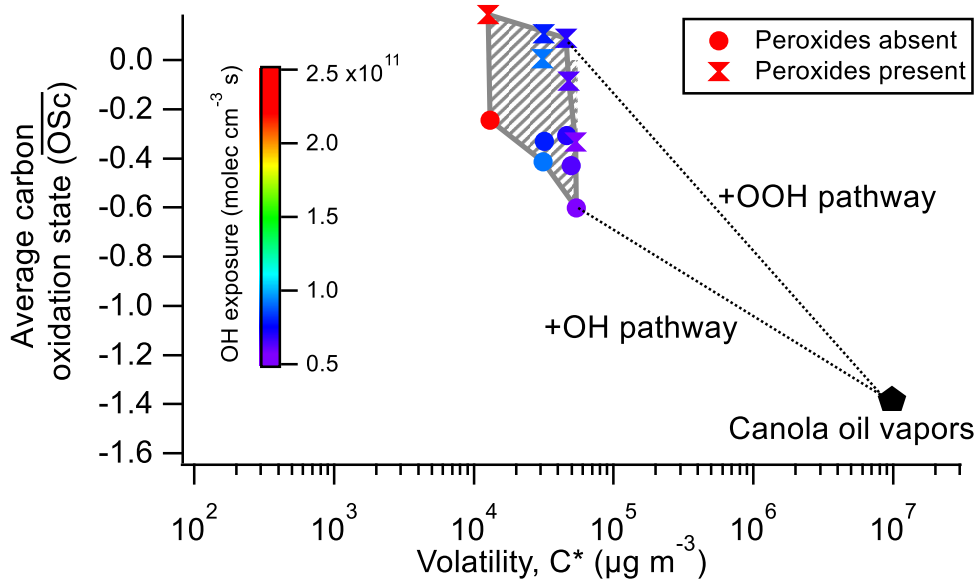

Figure S6. 2D-VBS for canola oil SOA upon photochemical aging in the atmosphere. The coloured markers represent bulk volatility of SOA under different photochemical aging conditions, while the black marker represents properties of canola oil vapors before oxidation. The shaded area corresponds to formation of SOA products with the uncertainty associated in identifying hydroxyl

and peroxide groups. If all hydroxyl groups were instead classified as peroxide groups, the $\overline{OSc}$ increases but the bulk volatility of SOA shows a minor decrease suggesting that classification of peroxide groups as hydroxyl groups has little effect on estimation of volatility.

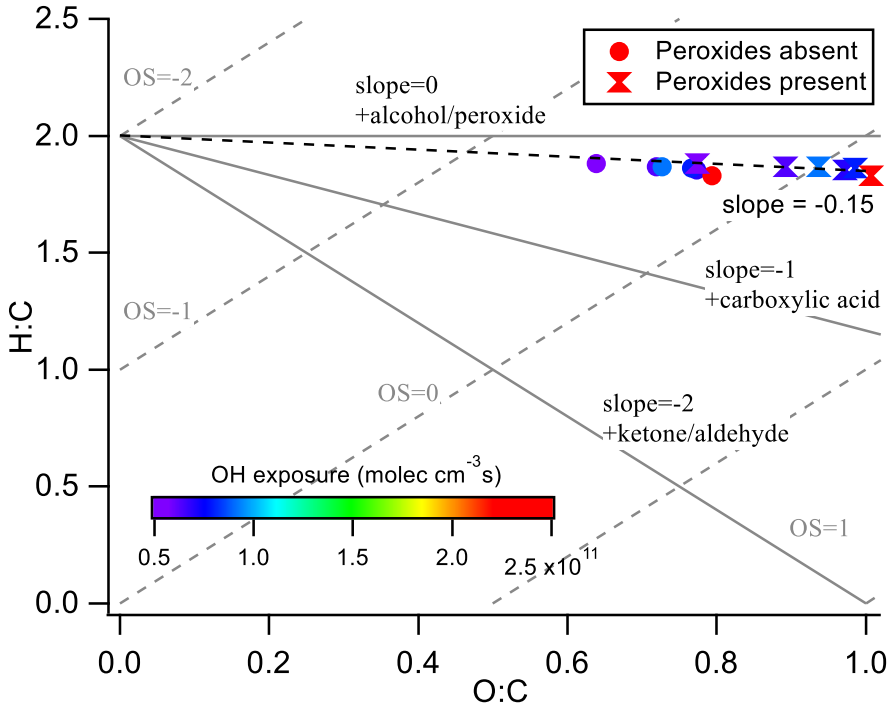

Figure S7. Van Krevelen diagram of canola oil SOA coloured by different OH exposure considering the presence of peroxides. The slope of -0.15 is observed when the formation of peroxides is considered in canola oil SOA similar to that of no-peroxides assumption (Fig. 4, main text).

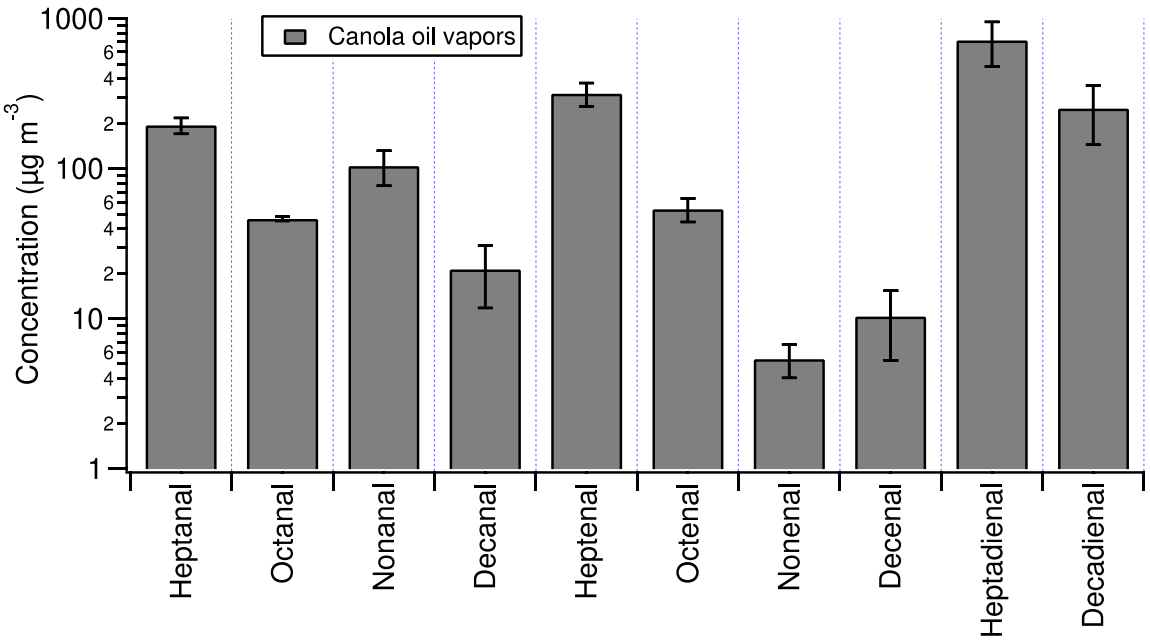

166

167 **Figure S8.** Concentration of different aldehydes quantified in this study.

168

169

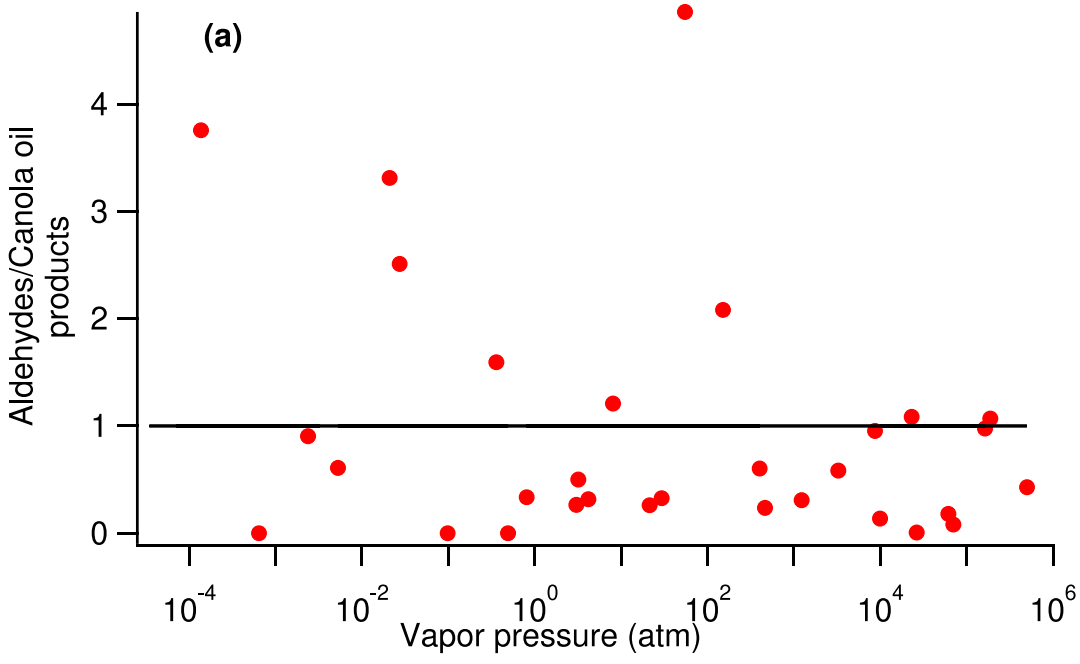

170

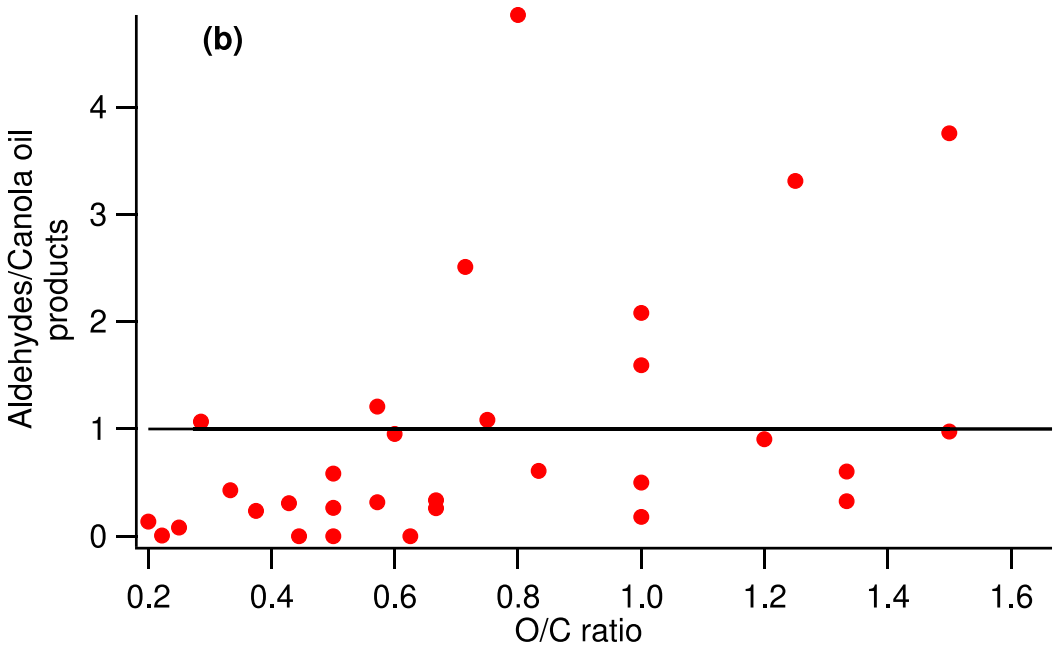

171

172

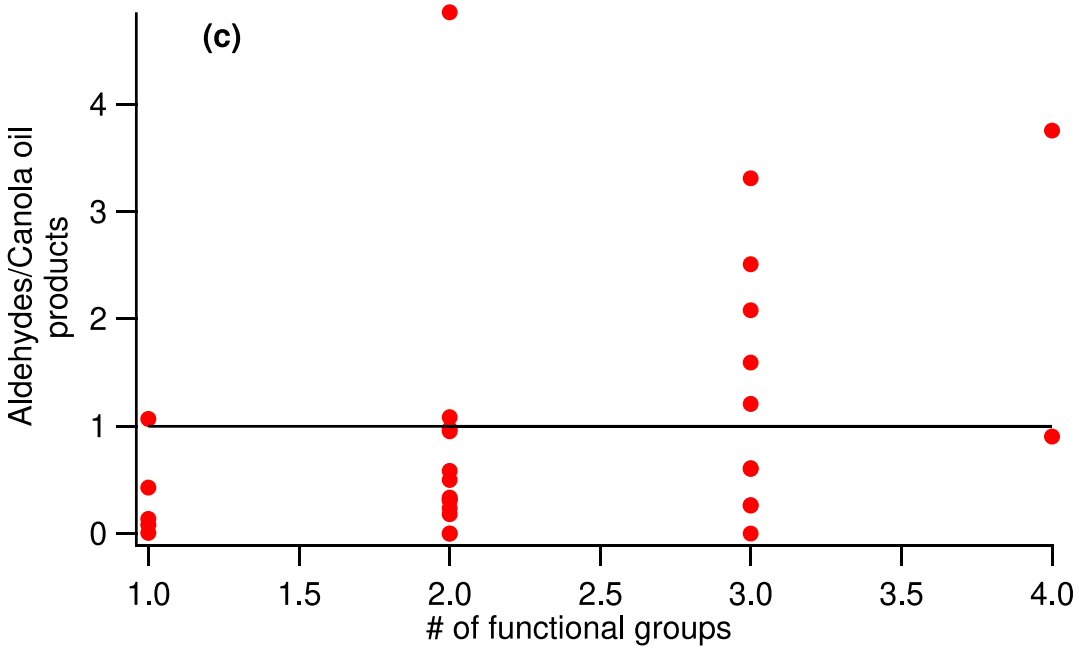

173

174

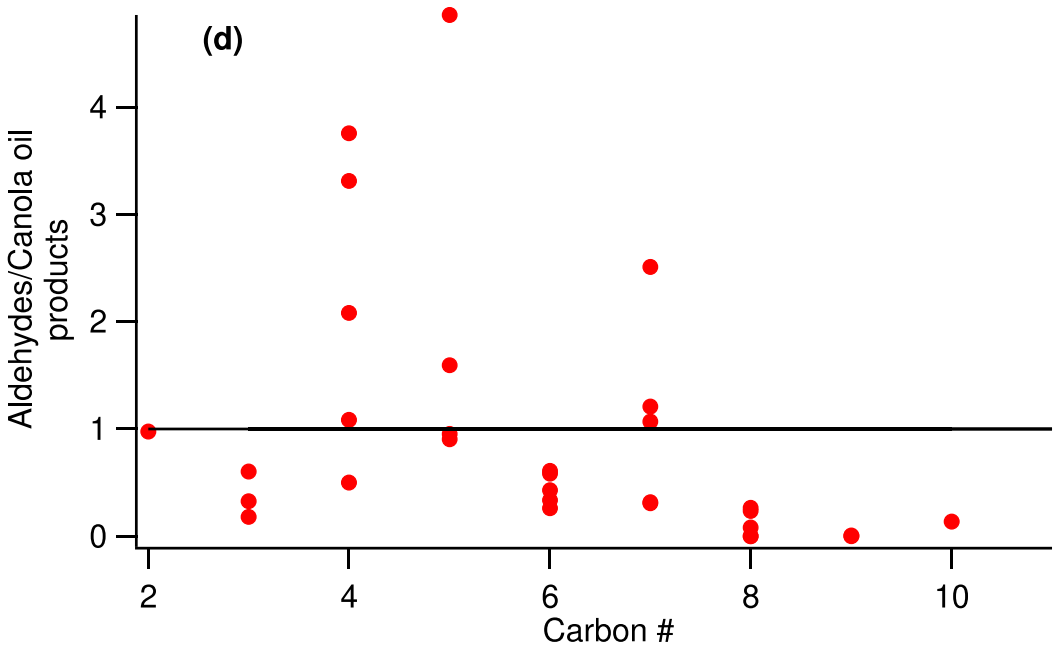

175

176 **Figure S9.** Comparison of the ratio of GC measured products from aldehydes photooxidation to canola oil photooxidation by
177 vapor pressure (a), O/C ratios (b), # of functional groups (c), and carbon # (d). In general, aldehydes SOA products are
178 underestimated for lower O/C ratios and number of functional groups, suggesting that canola oil SOA favors partitioning of more
179 oxygenated compounds than SOA formed from aldehydes.

180

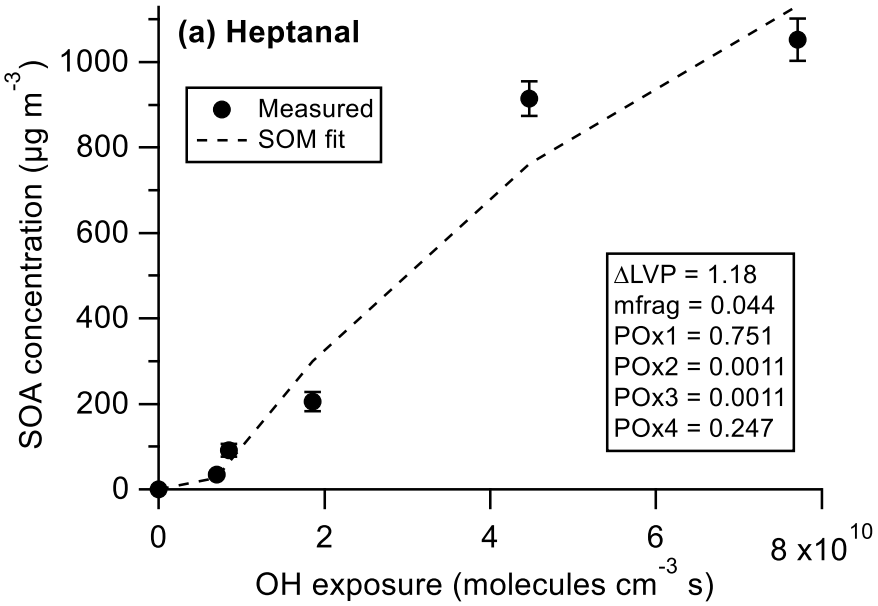

181

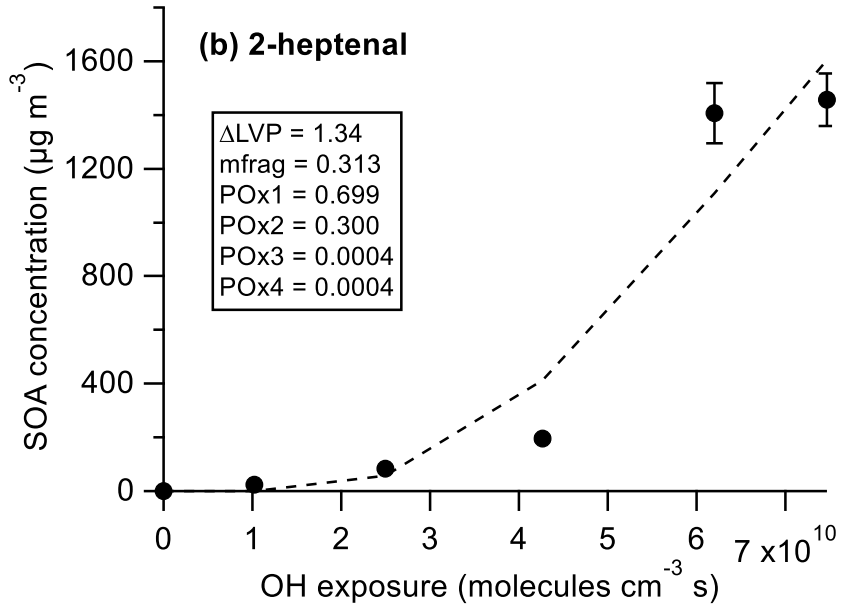

182

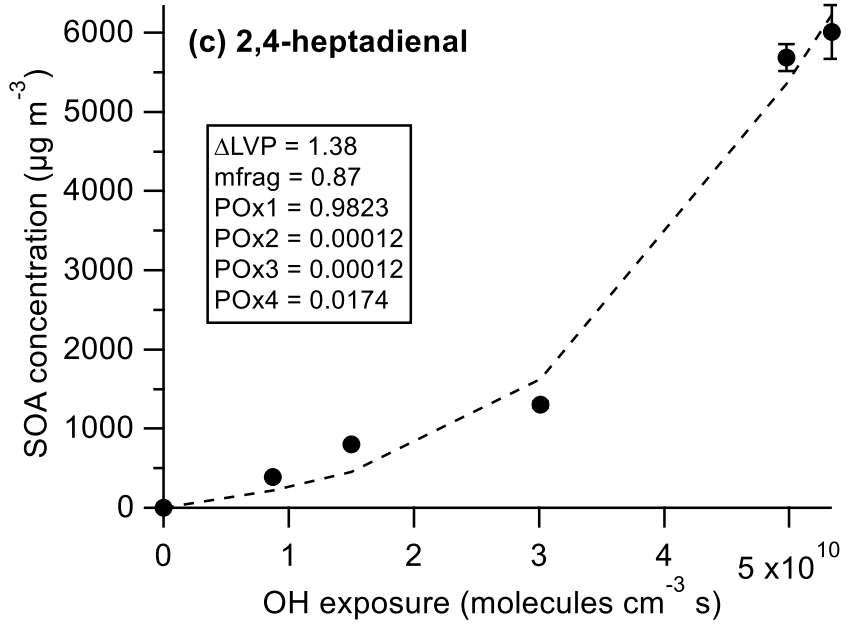

183

184 **Figure S10.** Estimation of SOM parameters by fitting SOA concentrations against OH exposure for heptanal (a), *trans*-2-heptenal
185 (b), and *trans*,*trans*-2,4-heptadienal (c) photooxidation.

186

References

Atkinson, R. and Arey, J.: Atmospheric Degradation of Volatile Organic Compounds, Chem. Rev., 103(12), 4605–4638, doi:10.1021/cr0206420, 2003.

Bilde, M., Svenningsson, B., Mønster, J. and Rosenørn, T.: Even-odd alternation of evaporation rates and vapor pressures of C3-C9 dicarboxylic acid aerosols, Environ. Sci. Technol., 37(7), 1371–1378, doi:10.1021/es0201810, 2003.

Davis, M. E., Gilles, M. K., Ravishankara, A. R. and Burkholder, J. B.: Rate coefficients for the reaction of OH with (E)-2-pentenal, (E)-2-hexenal, and (E)-2-heptenal, Phys. Chem. Chem. Phys., 9(18), 2240–2248, doi:10.1039/b700235a, 2007.

Gao, T.; Andino, J. M.; Rivera, C. C.; Marquez, M. F.: Rate Constants of the Gas-Phase Reactions of OH Radicals with trans-2-Hexenal, trans-2-Octenal, and trans-2-Nonenal, Int. J. Chem. Kinet., 41(7), 483–489, doi:10.1002/kin, 2009.

Kwok, E. S. C. and Atkinson, R.: Estimation of hydroxyl radical reaction rate constants for gas-phase organic compounds using a structure-reactivity relationship: An update, Atmos. Environ., 29(14), 1685–1695, doi:10.1016/1352-2310(95)00069-B, 1995.

Mao, J., Ren, X., Brune, W. H., Olson, J. R., Crawford, J. H., Fried, A., Huey, L. G., Cohen, R. C., Heikes, B., Singh, H. B., Blake, D. R., Sachse, G. W., Diskin, G. S., Hall, S. R. and Shetter, R. E.: Airborne measurement of OH reactivity during INTEX-B, Atmos. Chem. Phys., 9(1), 163–173, doi:10.5194/acp-9-163-2009, 2009.

Pankow, J. F. and Asher, W. E.: SIMPOL.1: A simple group contribution method for predicting vapor pressures and enthalpies of vaporization of multifunctional organic compounds, Atmos. Chem. Phys., 8(10), 2773–2796, doi:10.5194/acp-8-2773-2008, 2008.